Phase Transitions in a $LiMn_2O_4$ Nanowire Battery Observed by Operando Electron Microscopy

Soyeon Lee,[*,†,‡] Yoshifumi Oshima,[‡,§] Eiji Hosono,[∥] Haoshen Zhou,[*,∥] Kyungsu Kim,[⊥] Hansen M. Chang,[⊥] Ryoji Kanno,[⊥] and Kunio Takayanagi[‡,#]

[†]Quantum Nanoelectronics Research Center, Tokyo Institute of Technology, 2-12-1-H-52 Oh-okayama, Meguro-ku, Tokyo 152-8551, Japan, [‡]JST—CREST, 7-gobancho, Chiyoda-ku, Tokyo 102-0075, Japan, [§]School of Materials Science I, Japan Advanced Institute of Science and Technology, 1-1 M1-61 Asahidai, Nomi, Ishikawa 923-1292, Japan, [∥]Energy Technology Research Institute, National Institute of Advanced Industrial Science and Technology, 1-1-1 Umezono, Tsukuba, 305-8568, Japan, [⊥]Department of Electronic Chemistry, Tokyo Institute of Technology, 4259 G1-1 Nagatsuta, Midori-ku, Yokohama 226-8502, Japan, and [#]Department of Physics, Tokyo Institute of Technology, 2-12-1-H-51 Oh-okayama, Meguro-ku, Tokyo 152-8551, Japan

ABSTRACT Fast charge—discharge process has been reported to give a high capacity loss. A nanobattery consisting of a single $LiMn_2O_4$ nanowire cathode, ionic liquid electrolyte and lithium titanium oxide anode was developed for *in situ* transmission electron microscopy. When it was fully charged or discharged within a range of 4 V in less than half an hour (corresponding average C rate: 2.5C), Li-rich and Li-poor phases were observed to be separated by a transition region, and coexisted during whole process. The phase transition region moved reversibly along the nanowire axis which corresponds to the [011] direction, allowing the volume fraction of both phases to change. In the electron diffraction patterns, the Li-rich phase was seen to have the (100) orientation with respect to the incident electron beam, while the Li-poor phase had the (11$\bar{1}$) orientation. The orientation was changed as the transition region moved. However, the nanowire did not fracture. This suggests that a $LiMn_2O_4$ nanowire has the advantage of preventing capacity fading at high charge rates.

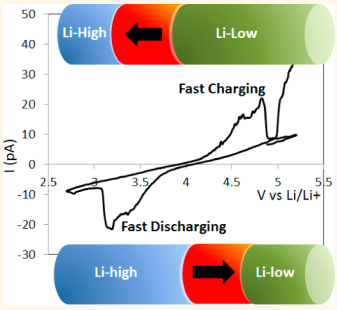

KEYWORDS: *in situ* TEM · lithium ion battery · phase transition · $LiMn_2O_4$ · nanowire · fast charge

Phase transition of electrode materials in lithium ion batteries inevitably occurs by lithium compositional change during charge—discharge processes. Understanding of the phase transition is a key to improve the battery performance. For example, the strain induced by the phase transition has been reported to cause capacity fading.[1−4] Most Li-alloy-based anode materials suffer from the strain due to the volume change during phase transition.[5−7]

Phase transition during charge—discharge processes has been investigated intensively using various methods: electrochemical methods,[8−13] such as transient methods or potential sweeping, X-ray diffraction,[14−16] and neutron diffraction.[17−19] Among these methods, *in situ* measurement is a powerful tool for elucidating the kinetics of the phase transition during charge—discharge processes.[15,20,21]

Recently, by *in situ* measurement, it has been suggested that high charge rates affect the kinetics of phase transition.[20,22] *In situ* XRD studies has reported that at high charge rates, the diffraction peaks corresponding to a metastable phase appeared, while at low charge rate, they did not appear in the $LiFePO_4$ crystals.[20,22] In our previous *in situ* transmission electron microscopy (TEM) study, we have found that a different type of phase transition occurred at the interface between the $LiMn_2O_4$ crystals and the electrolyte.[23] Even at the early discharge stage (3.9 V *vs* Li/Li^+), Li-excess tetragonal phase appeared at the interface region, though the tetragonal phase has been reported to appear below 3 V *vs* Li/Li^+.[4,14,15] This inhomogeneous lithium distribution is considered to be due to lithium accumulation at the interface at high charge rates.[23] Phase transition mechanism at high charge rates becomes more relevant as the demand for ever faster charge—discharge process increases.

A $LiMn_2O_4$ crystal is a promising cathode material because of its high reaction

* Address correspondence to lee.s.aj@m.titech.ac.jp, hs.zhou@aist.go.jp.

Received for review October 18, 2014 and accepted December 16, 2014.

Published online December 16, 2014
10.1021/nn505952k

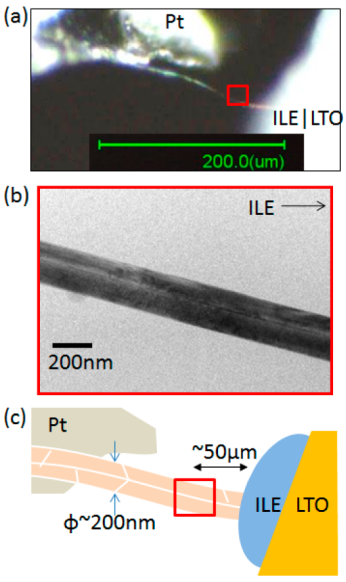

Figure 1. (a) Optical micrograph of a single-nanowire battery consisting of nanowire $LiMn_2O_4$ cathode, ionic liquid electrolyte (ILE) and $Li_4Ti_5O_{12}$ (LTO) anode. The observed area is marked by a red square. (b) TEM image of the observation area. (c) Schematic illustration of a single-nanowire battery. The white lines seen in the nanowire are crystalline domain boundaries.

voltage, abundant reserves of manganese, low cost, and nontoxicity.[24−26] The $LiMn_2O_4$ crystal is expected to be used for electric vehicles where charge−discharge proceeds rapidly. However, the $LiMn_2O_4$ crystal has been reported to lose its capacity relatively fast, compared with $LiCoO_2$ crystals, currently most used cathode materials.[25] One of the main reasons for capacity fading has been reported to be the strain due to the phase transition of two-phase reaction.[1,2] Unveiling capacity fading mechanism during phase transition of $LiMn_2O_4$ crystals would lead to new strategies for designing fast chargeable long-life $LiMn_2O_4$ based batteries.

In this study, we present the phase transition behavior inside a single $LiMn_2O_4$ nanowire cathode during a fast charge−discharge process by *in situ* TEM and diffraction observation. During the whole charge−discharge process, Li-rich and Li-poor phases coexisted, separated by a transition region. The transition region was observed to move along the nanowire reversibly during the charge−discharge process.

RESULTS

Single $LiMn_2O_4$ Nanowire Lithium Ion Battery. An optical micrograph of the nanowire battery is shown in Figure 1a. A single $LiMn_2O_4$ nanowire was supported by a platinum current collector and was put into contact with Ionic liquid electrolyte (ILE). The TEM image of the pristine nanowire in Figure 1b was taken in the area indicated by the red square in Figure 1a. The observed area was far from the $LiMn_2O_4$/ILE interface by about 50 μm, and the nanowire surface was observed not to be covered by ILE. The schematic illustration of the nanowire battery is shown in Figure 1c. The nanowire had a diameter of about 200 nm and had multiple crystalline domains. As illustrated in Figure 1c, a twin boundary, seen along the wire axis in Figure 1b, bounds the upper and lower sides of the nanowire. Some domain boundaries were observed across the wire, as indicated by the white lines in Figure 1c. The nanowire thickness gradually increased toward the center, where it was estimated to be about 140 nm thick by analyzing the transmission electron diffraction (TED) pattern as shown in Supporting Information Figure S1. TEM observation of the present nanowire battery was achieved simultaneously with cyclic voltammetry.

Current and Structure Evolution during Cyclic Voltammetry. The charge−discharge process was performed by cyclic voltammetry as shown in Figure 2a. (For convenience, cell voltages in this paper have been converted into potential *vs* Li/Li^+.) The voltage was swept from 5.2 to 2.7 V and then was increased back to 5.2 V. The voltage sweep speed was 0.55 mV/s. *In situ* TEM observation was performed from the first discharge process. In the first discharge process, the cathodic current started to increase around 3.8 V, and two cathodic current peaks appeared at 3.4 and 3.2 V. Then, the cathodic current decreased steeply at 3.1 V. The small residual cathodic current above the background level died out around 3.0 V. The nanowire battery was fully charged in 24 min, which corresponds to 2.5C. The linear background can be explained by the internal leak current of the nanowire battery. (Notice the extremely low current level.) In the sequential charge process, the anodic current started to increase above 4.2 V, and two anodic peaks appeared at 4.6 and 4.8 V. The anodic current decreased steeply at 4.9 V. The small residual anodic current above the background level died out around 5.0 V. The double cathodic (or anodic) current peaks correspond to the characteristic of the reaction of $LiMn_2O_4$ crystals in the 4 V range. The large polarization, which is voltage difference between the cathodic current peaks and the anodic current peaks, can be explained by the internal resistance of the nanowire battery and high charge rate.

The anodic and cathodic peak currents both recorded the same amounts of about 20 pA. By integrating the area demarcated by the current plot and background in the cyclic voltammogram, the charge capacity was estimated to be about 10 nC. It corresponds that all the lithium ions in a roughly 300-μm-long section of the nanowire was extracted. It indicated that our *in situ* TEM observation was performed at the area where lithium ions moved. The discharge capacity was also estimated to be about 10 nC, indicating that no significant capacity fading occurred.

Figure 2b shows a series of TEM images obtained during the discharge−charge process. We found that the "fringe-region", in which many dark fringes are

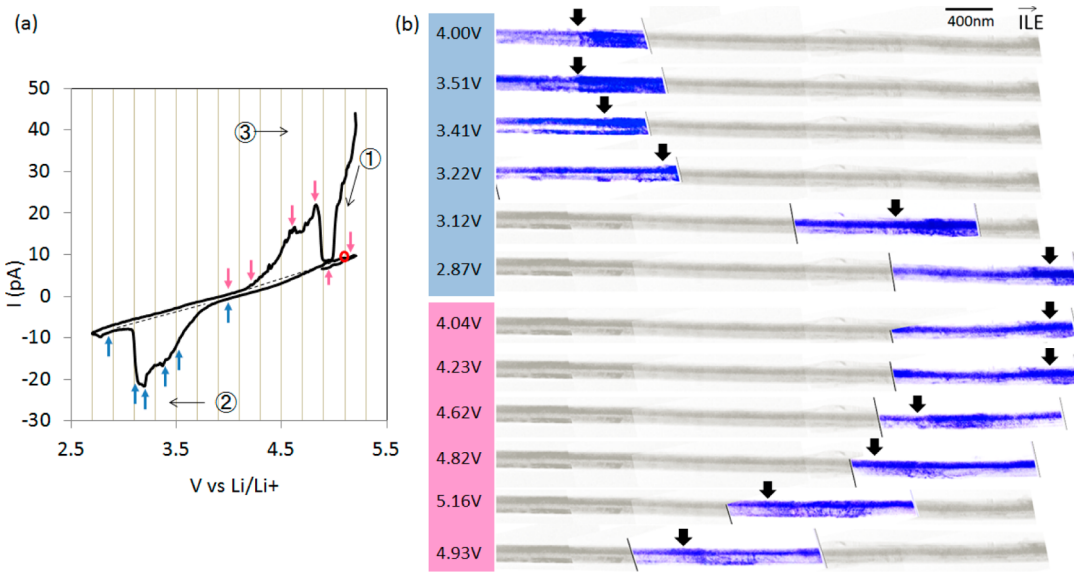

Figure 2. (a) Cyclic voltammogram (CV) of the nanowire battery with a single $LiMn_2O_4$ nanowire. Cyclic voltammetry was performed in order of the numbers (① → ② → ③) at a scan rate of 0.55 mV/s. The broken lines in the CV correspond to the background current level. Colored arrows correspond to TEM images in (b) (blue arrows: discharge; red arrows: charge). (b) A series of TEM images taken at different voltages (colored arrows in (a)). Blue images are the snapshots obtained at each voltage. Owing to the limited view area of individual snapshots, multiple TEM images are superimposed (gray) to highlight the position of the fringe-region. Black arrows indicate the left shoulder of the fringe-region. ILE was to the right of the nanowire, far from the observation area by 50 μm.

seen across the wire, moved along the wire axis toward the electrolyte during discharge process and moved back during charge process. As will be explained later, the left- and right-hand side of the fringe-region had different lithium composition.

The position change of the fringe-region was found to correlate closely with the cathodic and/or anodic current, as summarized in Figure 3a–c: These three plots show the time evolution of the applied voltage, circuit current, and fringe-region position, respectively. In the discharge process which started around 3.8 V and ended around 3.0 V, the fringe-region started to move around 3.4 V. It moved conspicuously around 3.2 V, and stopped around 2.8 V. The total displacement was about 4 μm during the discharging process;, while, in the charge process which started around 4.2 V and ended around 5.0 V, the fringe-region started to move in the opposite direction from about 4.2 V, moved conspicuously around 4.6 V and stopped around 5.1 V. The total displacement during the charge process was also about 4 μm, which is the same as that in the discharge process. Thus, the fringe-region started to move when the cathodic or anodic current increased, and moved when the cathodic or anodic current flowed.

The fringe-region tended to move slightly more toward the cathode collector after the cathodic or anodic current stopped. It moved for more than 900 s after the anodic current was stopped during the discharge process. During the charge process, it moved in the same direction for 600 s after the cathodic current was stopped (Figure 3c). The reason for these time lags will be discussed later. We found that, except for these time lags, the position change of the fringe-region correlated with the anodic or cathodic current. It means that it is correlated with the lithium diffusion. And also, the fringe-region was observed continually throughout the whole process.

Phase Transition Region between Li-Rich and Li-Poor Phases. Figure 4 shows a series of TEM images showing the movement of the fringe-region during the charge process. In the fringe-region, the pattern and/or contrast changed during the discharge–charge processes. The width of the fringe-region was about 900 nm on average, slightly fluctuating between 700 and 1100 nm during the process. Only the single fringe-region was observed within a roughly 10-μm-long section.

Figure 5 shows a TEM image recorded at 5.07 V after charge process. The transmission electron diffraction (TED) patterns were obtained at the four sites shown in Figure 5a. The TED pattern shows a cubic spinel structure in (100) orientation on the left-hand side of the fringe-region (Figure 5b), while, (11$\bar{1}$) orientation on the right-hand side (Figure 5e). They had different orientations with respect to the incident electron beam but they had the same [011] direction along the nanowire axis.

The TED pattern clearly shows {220} spots on the left-hand side of the fringe-region (Figure 5c), while it does not show {220} spots on the right-hand side (Figure 5). We modeled the $Li_xMn_2O_4$ structure, where lithium ions are randomly distributed at tetrahedral sites. As shown in Supporting Information Figure S2a,b, theoretical calculations, which took the sample

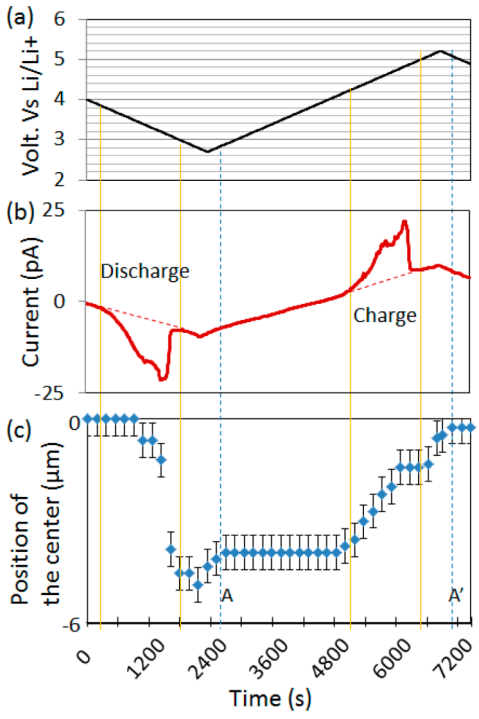

Figure 3. (a) Voltage variation during cyclic voltammetry of a single $LiMn_2O_4$ nanowire battery. (b) Current variation during cyclic voltammetry. The red broken lines indicate the background current level. (c) Position variation of the fringe-region with error bar as a function of time. Rightward displacements (toward ILE) are notated by negative value. The yellow solid lines over (a), (b), and (c) correspond to the starting or stopping point of the anodic or cathodic current. The blue broken lines correspond to the points when the movement of the fringe-region stopped.

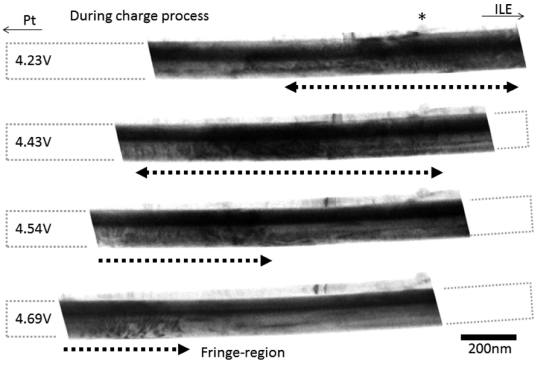

Figure 4. Series of TEM images of the fringe-region during charge process. The fringe-region is marked by a black dotted line arrow. The asterisk (*) indicates the protruding portion of the nanowire used to align the position of the TEM images. The outline of the nanowire is shown as gray dotted line.

thickness and observed orientation of the crystal into account, showed that the peak intensity of {220} spots was almost proportional to the lithium composition, while the peak intensity of {440} spots changed little. By comparing the experimental and calculated intensity ratio of {220} spots to {440} spots, the region on the left-hand side was determined to have a high lithium composition ($0.6 < x < 0.8$), whereas the region

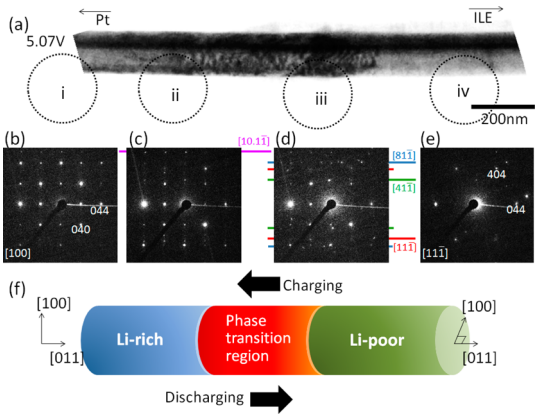

Figure 5. (a) TEM image of the fringe-region taken after the charge process, *i.e.*, at 5.07 V. The contrast consists of many dark and bright fringes across the nanowire section. TED patterns from the black broken circles i, ii, iii, and iv are shown in (b), (c), (d), and (e), respectively. The colored lines indicate orientations of the TED spots: the TED spots positioned on the colored line are to be observed when the viewing direction is aligned with the colored direction. All TED spots are from the domains in ⟨*n*11⟩ orientation, $n = \infty$, 10, 8, 4, and 1. (f) Schematic illustration of the structure and the movement of the fringe-region, *i.e.*, the phase transition region.

of the right-hand side, a low lithium composition ($x < 0.1$). (The details of the quantitative TED analysis are provided in the Supporting Information.) This indicates that Li-rich phase and Li-poor phase were separated by the fringe-region.

In the TED patterns of both Li-rich and Li-poor phases (Figure 5b,c), the {440} spots appeared at the equivalent distance from the origin within the error of 0.8%. The lattice constants between the Li-rich phase and Li-poor phase was not detectable. Since the difference of the lattice constant is more than 2.0% between $LiMn_2O_4$ and λ-MnO_2 phases, the Li-poor region cannot be explained simply by λ-MnO_2 phase. We consider that the Li-rich region is different from $LiMn_2O_4$ phase, and the Li-poor region is different from λ-MnO_2 phase at least.

In the fringe-region, the TED patterns (Figure 5c,d) show extra diffraction spots other than those due to the (100) and/or (11$\bar{1}$) orientations. On the left part of the fringe-region (Figure 5c), in addition to TED spots belonging to the (100) orientation, TED spots due to (10 1$\bar{1}$) orientation and TED spots due to (11$\bar{1}$) orientation appeared. On the right part (Figure 5d), the TED spots due to (81$\bar{1}$) orientation and TED spots due to (10 1$\bar{1}$), (41$\bar{1}$) and (11$\bar{1}$) orientation appeared (see Supporting Information Figure S4). These extra spots can be indexed by the cubic spinel phase in (*n*1$\bar{1}$) orientations ($n = \infty$, 10, 8, 4 and 1). This indicates that the fringe-region consists of several domains, whose orientations rotated from the (100) to the (11$\bar{1}$) orientation around the wire axis of the [011] direction.

Following the above TED analysis, we found that our nanowire has the structure illustrated in Figure 5f:

the left side of the fringe-region has the (100) orientation with a high composition of lithium ions, and the right side had the (11$\bar{1}$) orientation with a low lithium composition. In the "fringe-region", the orientation changes between these two. When we pay attention to the fringe-region movement during the charge process shown in Figure 4, it was found that the local structure of the Li-rich phase transformed into the Li-poor phase *via* the fringe-region. Therefore, we concluded that the fringe-region was the phase transition region between the Li-rich and Li-poor phases.

In summary, during the discharge−charge process, the phase transition region of Li-rich and Li-poor phases moved along the wire axis. The Li-rich phase was expanded in the discharge process (from 4 to 2.8 V), causing the transition region to move toward the electrolyte. While, in the charge process, the Li-poor phase was expanded causing the transition region to move toward the cathode collector. The phase transition region, which was observed continually throughout the whole discharge and charge processes, consists of several domains, whose orientations rotated around the wire axis of the [011] direction.

DISCUSSION

Phase Transition at High Charge Rate. The $Li_xMn_2O_4$ crystal has been reported to have two steps to be discharged from $x = 0$ to 1.[14,15,27] *In situ* XRD measurement with the discharge rate of C/10 (taking 10 h to be fully discharged) showed that phase transition occurred *via* a solid-solution reaction or two phase reaction depending on the lithium composition, x, in phase diagram:[14] In the range of 10−35% state of discharge (SOD), two phases with different lattice parameters (8.09 and 8.14 Å) coexisted, and the volume fraction of the larger-lattice-parameter phase increased linearly with increasing SOD. Above 35% SOD, only the larger-lattice-parameter phase remained, and the structure evolved through the phase transition that occurred *via* a solid-solution reaction, expanding the lattice parameter from 8.14 to 8.249 Å.

The Li-rich and Li-poor phases we observed differed from the reported two phases in the SOD range of 10−35%. In the present study, the Li-rich and Li-poor phases remained in the whole process of discharge, which covers the range of 0−100% SOD. One reason for this is considered to be the high charge rate, which affected the kinetics of the phase transition of the $Li_xMn_2O_4$ crystal. In our experiments, the nanowire battery was fully charged in 24 min, which corresponds to 2.5C on average. Under such a high charge rate, the equilibrium state could not be maintained during the discharge−charge process. In our previous study, we found that most lithium ions were accumulated in the vicinity of the surface of the $LiMn_2O_4$ nanowire cathode in the initial stage of the discharge process at the same high charge rate, indicating the unexpectedly inhomogeneous distribution of lithium ions.[23] Similarly, the high charge rate must induce inhomogeneous distribution of lithium ions inside a $LiMn_2O_4$ nanowire, and keep the two phases, namely, the Li-rich and Li-poor phases, during the whole process of discharge and charge in the present study.

We also considered the quantization and surface effect of $LiMn_2O_4$ nanowire, since $LiMn_2O_4$ particles having a crystallite size of 15 nm have been reported to undergo different phase transition process[12] due to the quantization and surface effect.[28] However, the present $LiMn_2O_4$ nanowire had a diameter of 200 nm, for which the quantization and surface effect is hardly expected. Also, it has been reported that the two steps, *i.e.* solid-solution reaction and two phases reaction, occurs during charge process in 130 nm-diameter $LiMn_2O_4$ nanowire, whose diameter is smaller than the present nanowire.[29] Thus, we concluded that the coexistence of the Li-rich and Li-poor phases throughout the whole process of charge or discharge can be attributed to the high charge rate.

Structure and Movement of the Phase Transition Region. In Figure 5c,d, all the observed diffraction spots could be indexed by the cubic spinel phase, especially in the (n1$\bar{1}$) orientations ($n = \infty$, 10, 8, 4 and 1). The orientation seems to be change in the order of (100) → (10 1$\bar{1}$) → (81$\bar{1}$) and (41$\bar{1}$), (11$\bar{1}$) → (11$\bar{1}$) from the left-hand to the right-hand side of the phase transition region. This indicates that in the phase transition region the domains were rotated from the (100) orientation to the (11$\bar{1}$) orientation around the wire axis of the [011] direction. The rotation mechanism could potentially involve a "*twisting*" since the orientation changed gradually from (100) to (11$\bar{1}$).

We have observed no twisted structure among the more than 100 pristine $LiMn_2O_4$ nanowires, but rather, only sharp domain boundaries having width narrower than several nanometers. Since the transition region appeared after the initial charge process from 5.2 V, its formation might be related to lithium movement. Given that the Li-rich domain has the (100) orientation and the Li-poor domain has the (11$\bar{1}$) orientation, initially a boundary between the (100) and (11$\bar{1}$) oriented domains would exist. The phase boundary would be trapped at the domain boundary under a nonequilibrium state, such as a high charge rate. The phase boundary should move by lithium insertion/extraction in spite of the different orientation between the two domains. In the first charge process, the domain orientation would start to be rotated by twisting of the structure, resulting in the formation of the twisted transition region.

In the TEM images, the phase transition region showed many fringes that were almost perpendicular to or slightly inclined with respect to the wire axis. The fringe-contrast of the TEM images would be originated by the strain and dislocations induced by the twisting.

Of course, the actual structure of the twisted transition region must be more complex since the number and shapes of the fringes in the TEM images changed gradually, as shown in Figure 4. To determine the structure of the twisted transition region exactly would require dark-field TEM observation with two-beam approximation.

As seen in Figure 3b,c, the fringe-region tended to move slightly toward the cathode collector after the cathodic or anodic currents stopped. This phenomenon can be understood as the redistribution of lithium ions upon the completion of lithium insertion or extraction into/from the nanowire. As long as the cathodic or anodic current flowed, the lithium composition would not reach its equilibrium value in the Li-rich and Li-poor regions. After the current stopped, lithium ions would continue to move from the Li-rich region to the Li-poor region to bring the local structure into an equilibrium state.

The phase transition region remained during the whole discharge−charge process. A large shear stress would be expected to occur at the boundary between the Li-rich region with (001) orientation and Li-poor region with (111) orientation. This stress might be accommodated by the one-dimensional shape of the nanowire, resulting in the formation of a roughly 900 nm-wide transition region. This suggests that the $LiMn_2O_4$ nanowire battery has the advantage of being able to prevent capacity fading at high charge rate.

CONCLUSION

We observed the phase transition behavior inside a $LiMn_2O_4$ nanowire cathode by *in situ* TEM. A nanobattery, which consisted of a single $LiMn_2O_4$ nanowire cathode, ionic liquid electrolyte and lithium titanium oxide anode, was fully charged (or discharged) in less than half an hour (corresponding average C rate: 2.5C). Throughout the fast charge−discharge process, Li-rich and Li-poor phases were separated by phase transition region. The transition region moved along the nanowire reversibly in order to transport lithium ions. Electron diffraction patterns revealed that the phase transition region connected the (100)-oriented Li-rich phase and the $(11\bar{1})$-oriented Li-poor phase, pointing to a twisted structure. The orientation changed as the transition region moved during the charge−discharge process. However, the nanowire did not physically fracture. This suggests that the $LiMn_2O_4$ nanowire offers the advantage of being able to prevent capacity fading at high charge rates.

EXPERIMENTAL SECTION

The nanobattery for *in situ* TEM observation was fabricated by the method reported previously.[23] The nanobattery consists of a nanowire $LiMn_2O_4$ cathode,[30] ionic liquid electrolyte (ILE), and $Li_4Ti_5O_{12}$ anode. Lithium *N*,*N*-bis(trifluoromethane sulfonyl)-imide (Li-TFSI) in *N*-methylpropylpiperidinium bis(trifluoromethanesulfonyl)imide (PP13TFSI) was used as electrolyte because of its low vapor pressure. In this study, a single $LiMn_2O_4$ nanowire was used as the cathode material. (Hereafter the battery will be referred to as "nanowire battery"). The nanowire battery was loaded onto our in-house developed electrical biasing double-tilt TEM holder, and was observed by an aberration-corrected TEM, R005 at 300 kV.[31] TEM images were obtained by bright field imaging with the high contrast objective aperture with a radius of 14 mrad, which is slightly larger than the {440} reflection of $LiMn_2O_4$ crystals in reciprocal space. TEM images and TED patterns were acquired by Ultrascan USC 1000 CCD camera (Model 894, Gatan, Inc.). During the TEM observation, the nanowire battery was charged and discharged by cyclic voltammetry. The voltage was scanned from 2.70 to 5.20 V *vs* Li/Li^+ at a scan rate of 0.55 mV/s. The measurement was performed by source-measurement unit, Keithley 2635A.

Conflict of Interest: The authors declare no competing financial interest.

Supporting Information Available: Details of quantitative TED analysis. This material is available free of charge *via* the Internet at http://pubs.acs.org.

Acknowledgment. This research was supported by JST-CREST.

REFERENCES AND NOTES

1. Shin, Y. J.; Manthiram, A. A. Microstrain and Capacity Fade in Spinel Manganese Oxides. *Electrochem. Solid Stat.* **2002**, *5*, A55–A58.
2. Shin, Y.; Manthiram, A. Factors Influencing the Capacity Fade of Spinel Lithium Manganese oxides. *J. Electrochem. Soc.* **2004**, *151*, A204–A208.
3. Gummow, R. J.; Kock, A. D.; Thackeray, M. M. Improved Capacity Retention in Rechargeable 4 V Lithium/Lithium−Manganese Oxide (Spinel) Cells. *Solid State Ionics* **1994**, *69*, 59–67.
4. Thackeray, M. M.; David, W. I. F; Bruce, P. G.; Goodenough, J. B. Lithium Insertion into Manganese Spinels. *Mater. Res. Bull.* **1983**, *18*, 461–472.
5. Larcher, D.; Beattie, S.; Morcrette, M.; Edstrom, K.; Jumasc, J.-C.; Tarascon, J.-M. Recent Findings and Prospects in the Field of Pure Metals as Negative Electrodes for Li-ion batteries. *J. Mater. Chem.* **2007**, *17*, 3759–3772.
6. Park, C.; Kim, J.; Kim, H.; Sohn, H. Li-alloy Based Anode Materials for Li Secondary Batteries. *Chem. Soc. Rev.* **2010**, *39*, 3115–3141.
7. Scrosati, B.; Garche, J. Lithium Batteries: Status, Prospects and Future. *J. Power Sources* **2010**, *195*, 2419–2430.
8. Wakihara, M.; Guohua, L.; Ikuta, H.; Uchida, T. The Spinel Phases $LiM_yMn_{2-y}O_4$ (M = Co, Cr, Ni) as the Cathode for Rechargeable Lithium Batteries. *Solid State Ionics* **1996**, *86−88*, 907–909.
9. Weppner, W.; Huggins, R. A. Determination of the Kinetic Parameters of Mixed-Conducting Electrodes and Application to the System Li_3Sb. *J. Electrochem. Soc.* **1977**, *124*, 1569–1578.
10. John Wen, C.; Boukamp, B. A.; Huggins, R. A.; Weppner, W. Thermodynamic and Mass Transport Properties of "LiAl". *J. Electrochem. Soc.* **1979**, *126*, 2258–2266.
11. Levi, M. D.; Gamolsky, K.; Aurbach, D.; Heider, U.; Oesten, R. Evidence for Slow Droplet Formation during Cubic-to-Tetragonal Phase Transition in $Li_xMn_2O_4$ Spinel. *J. Electrochem. Soc.* **2000**, *147*, 25–33.
12. Okubo, M.; Mizuno, Y.; Yamada, H.; Kim, J.; Hosono, E. Fast Li-ion Insertion into Nanosized $LiMn_2O_4$ without Domain Boundaries. *ACS Nano* **2010**, *4*, 741–752.

13. Bard, A. J.; Faulkner, L. R. *Electrochemical Methods-Fundamentals and Applications*, 2nd ed,; John Wiley & Sons: New York, 2001; p 226.
14. Eriksson, T.; Hjelm, A.-K.; Lindbergh, G.; Gustafsson, T. Kinetic Study of $LiMn_2O_4$ Cathodes by *in Situ* XRD with Constant-Current Cycling and Potential Stepping. *J. Electrochem. Soc.* **2002**, *149*, A1164–A1170.
15. Liu, W.; Kowal, K.; Farrington, G. C. Mechanism of the Electrochemical Insertion of Lithium into $LiMn_2O_4$ Spinels. *J. Electrochem. Soc.* **1998**, *145*, 459–465.
16. Delmas, C.; Maccario, M.; Croguennec, L.; Le Cras, F.; Weill, F. Lithium Deintercalation in $LiFePO_4$ Nanoparticles *via* a Domino-Cascade Model. *Nat. Mater.* **2008**, *7*, 665–671.
17. Nishimura, S.; Kobayashi, G.; Ohoyama, K.; Kanno, R.; Yashima, M.; Yamada, A. Experimental Visualization of Lithium Diffusion in Li_xFePO_4. *Nat. Mater.* **2008**, *7*, 707–711.
18. David, W.; Thackeray, M.; Picciotto, L.; Goodenough, J. Structure Refinement of the Spinel-related Phases $Li_2Mn_2O_4$ and $Li_{0.2}Mn_2O_4$. *J. Solid State Chem.* **1987**, *67*, 316–323.
19. Tateishi, K.; Boulay, D.; Ishizawa, N.; Kawamura, K. Structural Disorder along the Lithium Diffusion Pathway in Cubically Stabilized Lithium Manganese Spinel II. Molecular Dynamics Calculation. *J. Solid State Chem.* **2003**, *174*, 175–181.
20. Orikasa, Y.; Maeda, T.; Koyama, Y.; Murayama, H.; Fukuda, K.; Tanida, H.; Arai, H.; Matsubara, E.; Uchimoto, Y.; Ogumi, Z. Direct Observation of a Metastable Crystal Phase of Li_xFePO_4 under Electrochemical Phase Transition. *J. Am. Chem. Soc.* **2013**, *135*, 5497–5500.
21. Reimers, J. N.; Dahn, J. R. Electrochemical and *in Situ* X-Ray Diffraction Studies of Lithium Intercalation in Li_xCoO_2. *J. Electrochem. Soc.* **1992**, *139*, 2091–2097.
22. Liu, H.; Strobridge, F. C.; Borkiewicz, O. J.; Wiaderek, K. M.; Chapman, K. W.; Chupas, P. J.; Grey, C. P. Capturing Metastable Structures during High-rate Cycling of $LiFePO_4$ Nanoparticle Electrodes. *Science* **2014**, *344*, 1252817.
23. Lee, S.; Oshima, Y.; Hosono, E.; Zhou, H.; Kim, K.; Chang, H. M.; Kanno, R.; Takayanagi, K. *In Situ* TEM Observation of Local Phase Transformation in a Rechargeable $LiMn_2O_4$ Nanowire Battery. *J. Phys. Chem. C* **2013**, *117*, 24236–24241.
24. Thackeray, M. M.; Johnson, P. J.; Picciotto, L. A.; Bruce, P. G.; Goodenough, J. B. Electrochemical Extraction of Lithium from $LiMn_2O_4$. *Mater. Res. Bull.* **1984**, *19*, 179–187.
25. Thackeray, M. M. Spinel Electrodes for Lithium Batteries. *J. Am. Ceram. Soc.* **1999**, *82*, 3347–3354.
26. Tarascon, J. M.; Armand, M. Issues and Challenges Facing Rechargeable Lithium Batteries. *Nature* **2001**, *414*, 359–367.
27. X. Sun, X.; Yang, X. Q.; Balasubramanian, M.; McBreen, J.; Xia, Y.; Sakai, T. *In Situ* Investigation of Phase Transitions of $Li_{1+y}Mn_2O_4$ Spinel during Li-Ion Extraction and Insertion. *J. Electrochem. Soc.* **2002**, *149*, A842–A848.
28. Wagemaker, M.; Mulder, F. M.; Van der Ven, A. The role of surface and interface energy on phase stability of nano-sized insertion compounds. *Adv.mater.* **2009**, *21*, 2703–2709.
29. Kim, D.; Muralidharan, P.; Lee, H.; Ruffo, R.; Yang, Y.; Chan, C. K.; Peng, H.; Huggins, R. A.; Cui, Y. Spinel $LiMn_2O_4$ Nanorods as Lithium Ion Battery Cathodes. *Nano Lett.* **2008**, *8*, 3948–3952.
30. Hosono, E.; Kudo, T.; Honma, I.; Matsuda, H.; Zhou, H. Synthesis of Single Crystalline Spinel $LiMn_2O_4$ Nanowires for a Lithium Ion Battery with High Power Density. *Nano Lett.* **2009**, *9*, 1045–1051.
31. Sawada, H.; Tanishiro, Y.; Ohashi, N.; Tomita, T.; Hosokawa, F.; Kaneyama, T.; Kondo, Y.; Takayanagi, K. STEM Imaging of 47-pm-separated Atomic Columns by a Spherical Aberration-Corrected Electron Microscope with a 300-kV Cold Field Emission Gun. *J. Electron. Microsc.* **2009**, *58*, 357–361.